Large cryogenic magnetocaloric effect in the blocking state of $GdAl_2/Al_2O_3$ nanocapsules

S. Ma, W. F. Li, D. Li, D. K. Xiong, N. K. Sun, D. Y. Geng, W. Liu, and Z. D. Zhang
Shenyang National Laboratory for Material Science, Institute of Metal Research, and International Centre for Material Physics, Chinese Academy of Sciences, 72 Wenhua Road, Shenyang 110016, China

(Received 11 January 2007; revised manuscript received 7 September 2007; published 1 October 2007)

The nanocapsules with crystalline cores of $GdAl_2$ compound and shells of amorphous Al_2O_3 were prepared by evaporating Gd_xAl_{100-x} ($x=50$, 60, 70, 80, and 90) alloys using a modified arc-discharge technique. The morphologies, average sizes, lattice constants, and surface characteristics of $GdAl_2/Al_2O_3$ nanocapsules were studied in detail by means of x-ray diffraction, energy dispersive spectroscopy, x-ray photoelectron spectroscopy, and high-resolution transmission electron microscopy. The formation mechanism of the nanocapsules was analyzed in detail. The differences in Curie temperatures and anisotropy constants of these nanocapsules were discussed with respect to their different structural characteristics. From 180 to 5 K, the magnetic entropy change of the $GdAl_2/Al_2O_3$ nanocapsules continuously increases with decreasing temperature T and rapidly enhances when the temperature tends to 5 K. The largest entropy change $-\Delta S$ at 7.5 K can respectively reach 18.02, 18.71, and 31.01 J kg^{-1} K^{-1} by varying the magnetic field from 7 to 1 T for the nanocapsules synthesized by arc-discharging $Gd_{70}Al_{30}$, $Gd_{80}Al_{20}$, and $Gd_{90}Al_{10}$ alloys. The appearance of a large entropy change at low temperatures was ascribed to a lower anisotropy energy barrier and a high magnetic-moment density of the nanocapsules. The linear relation between the magnetic entropy change and the reciprocal of the temperature ($1/T$) was discussed in terms of superparamagnetism and magnetocaloric theory.

DOI: 10.1103/PhysRevB.76.144404 PACS number(s): 75.30.Sg, 75.20.−g, 75.30.Gw, 75.50.Tt

I. INTRODUCTION

The magnetocaloric effect (MCE) is generally recognized as a conversion of the magnetic energy of a magnetic substance into thermal energy in a varying dc magnetic field, whose magnitude can be judged indirectly by the isothermal magnetic entropy change in the magnetization process.[1] Extensive researches have been performed to utilize this effect as an environment-friendly technology in the refrigeration field, in order to replace the traditional gas compression and/or expansion technology.[2–5] Up to now, MCE has been practically applied in magnetic refrigeration devices in a low-temperature range ($T<20$ K) by using the paramagnetic salt $Gd_3Ga_5O_{12}$.[6] Theoretically, the higher the density of magnetic moments and their spin number, the greater the cooling power of a refrigerant.[7] Based on the calculation of superparamagnetic theory, McMichael *et al.* predicted that nanomagnets would have a larger magnetic entropy change because of the existence of a large magnetic-moment density in a single magnetic particle.[8] Subsequently, the prediction was soon proven by Yamamoto *et al.* in Fe_2O_3-Ag nanocomposites.[9,10] In order to overcome the oxidation of magnetic nanoparticles, more nanocomposites were studied.[11–13] However, the nonmagnetic substrate decreased intensively the density of magnetic moments, which hindered the enhancement of the entropy change.[11–13] Subsequently, to further enhance the MCE of nanomagnets, great efforts have been made to increase the moments of a particle by increasing atomic moments.[14–17] Especially, the entropy changes of 6 and 17.6 J kg^{-1} K^{-1} were respectively achieved at 8 and 6 K with the field changes of 3 and 7 T for anisotropic superparamagnetic Fe_8 and Fe_{14} molecular clusters, but the complicated preparation limits their practical application.[17,18] Nevertheless, more endeavors were focused on improving MCE by using nanomagnets in their superparamagnetic state. It is not neglected that the nanoparticles with higher energy barrier would have higher blocking temperature, which would limit their application in low temperatures, because the blocking state is detrimental for MCE of the nanoparticles. Therefore, for the nanoparticles with large atomic moments and low energy barriers, the magnetic moments may easily overcome the barriers to change their alignments to acquire the large entropy change at low temperatures. To date, little work has been done to discuss the potentially high MCE of the nanoparticles, with a high moment density and a low energy barrier, and to exploit a new type of nanomagnets responsible for this property.

$GdAl_2$ intermetallic compound crystallizes in the cubic $MgCu_2$-type structure (C15 Laves phase), in which Gd ions form a sublattice of diamond type and the corresponding nearest neighbors are Al atoms occupying corner-sharing tetrahedral networks. In one $GdAl_2$ unit cell, there are 16 Al sites forming four corner-sharing tetrahedrons with point symmetry $\bar{3}m$, while the point symmetry of Gd sites belongs to the cubic group.[19] In agreement with predictions of the Rudermann-Kittel-Kasuya-Yosida model of indirect exchange, the $GdAl_2$ compound orders ferromagnetically with its paramagnetic Curie temperature of 172 K.[20,21] Generally, the long-range ferromagnetic order of $GdAl_2$ originates from the following: the local Gd $4f$ electrons polarize the conduction electrons of $6s$, $6p$, and $5d$ orbitals in Gd and $3s$ and $3p$ orbitals in Al through local exchange interactions, and the dominant interaction between the $4f$ and $5d$ states is positive so that the corresponding spin moments are always parallel.[22,23] Although the gadolinium atoms provide a fairly strong exchange field to result in a high Curie temperature, they contribute very little anisotropy (because of its orbital momentum $L=0$) and, consequently, the anisotropy field of pure $GdAl_2$ is relatively small among RAl_2 ($R\equiv$rare earths).[24] Importantly, when the size of the crystalline $GdAl_2$

 ©2007 The American Physical Society

decreases to nanoscale, it will turn from the ferromagnetic state into the superparamagnetic state. Therefore, the $GdAl_2$ nanoparticles, with large atomic moments for its total angular momentum of $J=7/2$ and low anisotropy energy barriers, will serve as the candidate for enhancing their MCE in the blocking state.

Although there have been many reports on the nanoparticles (or nanocapsules), due to difficulties in sample preparations because of the high activity of rare-earth elements, experimental work on the nanoparticles of rare-earth-transition-metal (RT) compounds (or the nanocapsules with RT compounds as cores) are scarcely seen.[25–34] Based on the modified arc-discharge technique developed in our previous work,[33] recently, we successfully synthesized dispersive $GdAl_2$ nanocapsules with $GdAl_2$ cores and nonmagnetic Al_2O_3 shells, and the large magnetic entropy change of 14.5 J kg^{-1} K^{-1} was acquired at 5 K from the nanocapsules.[25] The formation of the Al_2O_3 shells is very important to prevent the severe oxidation of rare-earth atoms like Gd, which usually happens easily, and thus, it is crucial for the formation of nanocapsules with RT compounds like $GdAl_2$ as cores. This advance in technology of synthesizing the *R*-containing nanocapsules provides many chances for a detailed investigation on the structure and physical properties of different types of novel nanocapsules. In this paper, the structures, magnetic properties, and magnetic entropy change of the $GdAl_2/Al_2O_3$ nanocapsules, synthesized by evaporating Gd-Al alloys with various compositions, are systematically investigated. One of the purposes of this work is to study in detail the formation mechanism of the nanocapsules with RT intermetallic compound, also in order to realize larger MCE. The large magnetic entropy change of 31.01 J kg^{-1} K^{-1} is achieved at 7.5 K by varying the magnetic field from 7 to 1 T for the $GdAl_2/Al_2O_3$ nanocapsules synthesized by arc-discharging $Gd_{90}Al_{10}$ alloy. Another purpose of the present work is to uncover the mechanism of the large magnetic entropy change in the $GdAl_2/Al_2O_3$ nanocapsules. It is found that different from the enhancement of MCE by the first-order or second-order phase transition,[27] the large magnetic entropy change in the present system comes from the effect of low anisotropy energy barriers, reducing the hindrance effect on the fluctuation of magnetization in the blocking-state $GdAl_2/Al_2O_3$ nanocapsules. The linear relation between the entropy change and the reciprocal of the temperature $(1/T)$ in the blocking state is uncovered, which is discussed in terms of superparamagnetism and magnetocaloric theory. In addition, the experimental results verify the theoretic prediction that the entropy change increases continuously with decreasing temperature for isotropic nanoclusters in the superparamagnetic state.

The paper is arranged as follows. The experimental details are given in Sec. II. The phase constitutions, elements analysis, particle morphologies, surface characteristics, crystalline image, and the formation mechanism of the $GdAl_2/Al_2O_3$ nanocapsules are studied in detail in Sec. III A. In Sec. III B, different magnetic characteristics in different temperature ranges and the variation of the Curie temperatures for the $GdAl_2/Al_2O_3$ nanocapsules with different compositions are discussed. Especially, the MCE of the $GdAl_2/Al_2O_3$ nanocapsules and the temperature dependence of the magnetic entropy change from 5 to 180 K are discussed in detail, in terms of superparamagnetic theory and magnetocaloric theory. The summary is given in Sec. IV.

II. EXPERIMENTAL DETAILS

The Gd_xAl_{100-x} alloy ingots with $x=50$, 60, 70, 80, and 90 were fabricated by arc-melting Gd and Al bulks with 99.8 wt % purity four times under a high purity argon atmosphere. The $GdAl_2/Al_2O_3$ nanocapsules were prepared by the modified arc-discharge method analogous to that employed in our previous work,[28–30] in which the cathode tungsten needle with diameter of 3 mm maintained a distance of 2–3 mm with the anode of Gd_xAl_{100-x} alloy ingots. When the vacuum of the arc-discharge chamber reached 6.5×10^{-3} Pa, Ar and H_2 were introduced into the chamber to reach 2.0×10^4 and 2.0×10^3 Pa, respectively. Then the arc was generated and the discharge current was maintained at 80 A for 5 h. After passivation in argon for 16 h, the nanocapsules were collected from the top of the chamber.

The phases made up of as-prepared nanocapsules were identified by powder x-ray diffraction (XRD) with Cu $K\alpha$ ($\lambda=0.154\,056$ nm) radiation on a Rigaku D/max-2000 diffractometer at a voltage of 50 kV and a current of 250 mA with a graphite crystal monochromator. The elements' ratio in the as-prepared nanocapsules was determined by energy dispersive spectroscopy (EDS) analysis. The size distribution, morphology, and crystalline images were investigated by a high-resolution transmission electron microscope (HR-TEM JEOL-2010) with emission voltage of 200 kV. X-ray photoelectron spectroscopy (XPS) measurement was performed on ESCALAB-250 with a monochromatic x-ray source (aluminum $K\alpha$ line of 1486.6 eV) to characterize the valence of surface atoms of the nanocapsules with depth from 0 to 10 nm. The nanocapsules were pressed together and mixed with liquid paraffin through heating by hot water, and then condensed by cooling, in order to avoid the rotation of the particles toward the direction of the applied field during magnetic measurements. The magnetic properties were measured by a superconducting quantum interference device (MPMS-7, Quantum Design) magnetometer.

III. RESULTS AND DISCUSSION

A. Analysis of structure and the formation mechanism

Figure 1 presents XRD patterns of five samples of the nanocapsules denoted as A, B, C, D, and E, which were prepared by arc-discharging the anode Gd_xAl_{100-x} with, respectively, different Gd percentages ($x=50$, 60, 70, 80, and 90). With the increase of the Gd content x in the anode alloys, the phase component of the nanocapsules is changed from fcc Al in samples A and B, and $GdAl_2$ in samples C and D, to the coexistence of $GdAl_2$ and fcc Gd in sample E. According to previous work,[25] the formation of different phases can be explained by the ratio of the metal atoms in the chamber. In the arc-discharge process, the metal atoms evaporated from the anodes with different compositions into the chamber, in which the atoms with a high activity reacted rapidly and nucleated through the rapid energy exchange.[32]

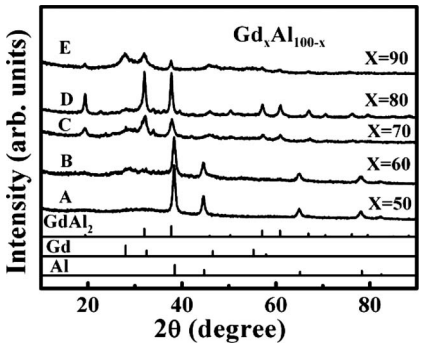

FIG. 1. X-ray diffraction patterns of the nanocapsules prepared by arc-discharging Gd_xAl_{100-x} (x=50–100) alloys.

In essence, the boiling point (or evaporation pressure) of metals determines the amount of evaporated atoms. With its boiling point of 2740 K, Al was more easily evaporated than Gd with a boiling point of 3539 K. As a result, more Al atoms evaporated into the chamber in unit time. From EDS results (Fig. 2), it is suggested that the ratio of the Gd and Al atoms controlled the formation of phases in the five nanocapsules. For nanocapsules A (B), the ratio of 1:30 (1:16) for Gd:Al indicates the predominant amount of Al, which results in the formation of fcc Al. Only when the Gd content is 70 at. % in the anode can the Gd:Al ratio reach 1:2.8 in nanocapsules C, which leads to the disappearance of fcc Al and the appearance of $GdAl_2$. When the ratio of Gd to Al reaches 1.25:1 in nanocapsules E, besides the formation of $GdAl_2$, the excessive Gd atoms favor the formation of the high-temperature phase fcc Gd. Therefore, the phases in the present nanocapsules are determined by the boiling points and the contents of the metals in the anode. Furthermore, it is noteworthy that only $GdAl_2$ and fcc Gd appear in samples C–E, although there are at least five kinds of compounds in the Gd-Al phase diagram. This can be explained by the fact that $GdAl_2$ and fcc Gd have the largest formation Gibbs energy and the highest decomposition temperatures of 1798 and 1586 K, respectively, among all the Gd-Al binary compounds. It is also noteworthy that as a high-temperature phase stable above 1508 K, the existence of fcc Gd at room temperature can be attributed to the lower surface energy of nanoscale particles[32] and the easy formation of the nanoparticles with metastable phases in the nonequilibrium processes.[31]

Another important information is that the atomic substitution induces the change of lattice constants of fcc Al and

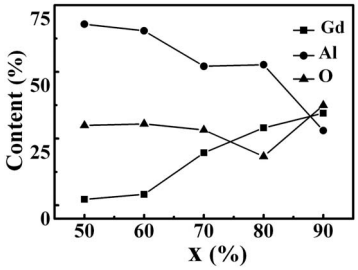

FIG. 2. Compositions of nanocapsules A–E as a function of Gd content x in the anode.

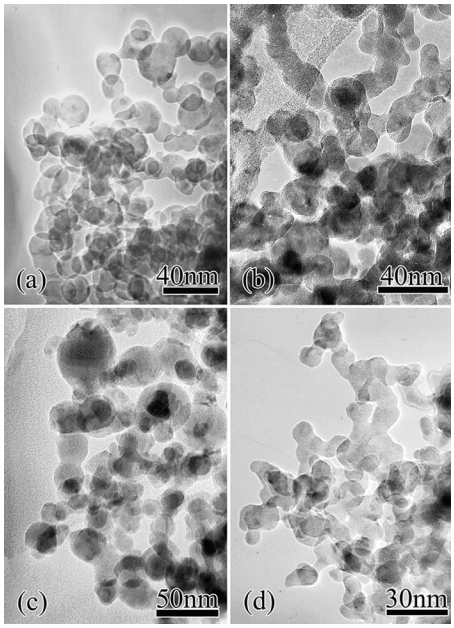

FIG. 3. TEM images showing morphologies of the nanocapsules of (a) sample B, (b) sample C, (c) sample D, and (d) sample E.

$GdAl_2$. According to the XRD pattern, the lattice constants of $GdAl_2$ are 0.7871, 0.7894, 7.9111, and 0.7899 nm for samples C, D, E, and the standard value, respectively. It indicates that for samples C and D, Al atoms with smaller atomic radius replace Gd position, making the lattice shrink, and the lattice tends to the standard state with the decrease of Al atoms; however, for sample E, excessive Gd atoms with larger atomic radius occupy part of the Al sites, causing the lattice expansion.

By transmission electron microscopy (TEM) investigation, the morphologies and size distribution of nanocapsules B–E are shown in Figs. 3 and 4. The nanocapsules are of irregular spherical shape as illustrated in Fig. 3. From Fig. 4, the size distribution of samples B–E are 12–30, 10–28, 8–35, and 9–22 nm, and the average diameters of the four nanocapsules are 22, 19, 24, and 17 nm (15 nm, Gd) respectively, in agreement with the results calculated from XRD patterns.

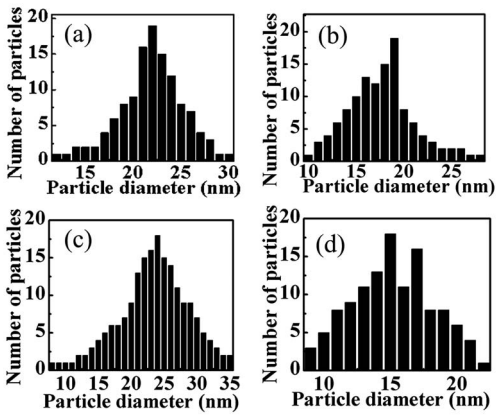

FIG. 4. Particle size distribution of (a) sample B, (b) sample C, (c) sample D, and (d) sample E.

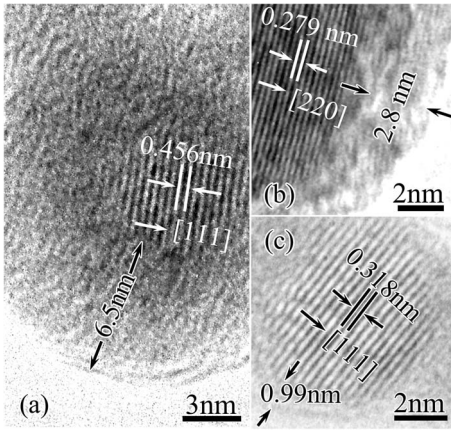

FIG. 5. HRTEM images of the $GdAl_2$ nanocapsules in (a) sample C, (b) sample D, and the HRTEM image of Gd nanocapsules in (c) sample E.

The HRTEM images of nanocapsules C–E are shown in Fig. 5. The typical core-shell structure with crystalline cores and amorphous shells can be observed. The *d* spacings of 0.456 and 0.279 nm correspond to the characteristic lattice distance of (111) and (220) of the $GdAl_2$ compound, which reveals that the crystalline cores are $GdAl_2$ for nanocapsules C and D [Figs. 5(a) and 5(b)]. The determination of the fcc Gd core of the nanocapsules in sample E can also be confirmed by the characteristic interplane spacing of 0.318 nm of (111) [Fig. 5(c)].

XPS patterns of Al $2p$ 3/2 in nanocapsules D with etching depths of 0, 2, 5, and 10 nm are presented in Fig. 6. With increasing etching depth, the binding energy peaks are 74.4, 74.1, 73.6, and 73.9 eV, respectively. Because 74.4 eV is consistent with the binding energy of Al $2p$ 3/2 in Al_2O_3,[34] the shells of nanocapsules D can be identified as Al_2O_3. The formation of Al_2O_3 shells can be attributed to the light atomic mass and comparatively lower melting point for Al atoms, which made them more easily absorbed on the surface of $GdAl_2$ cores and condensed in the arc-discharge process, and the surface Al atoms were oxidized subsequently in air. On the other hand, the shells of the $GdAl_2/Al_2O_3$ nanocapsules C are thicker than those of D and E, which reveals that more excessive Al atoms are prone to accumulate on the surface of $GdAl_2$ core to construct the shells (Fig. 5).

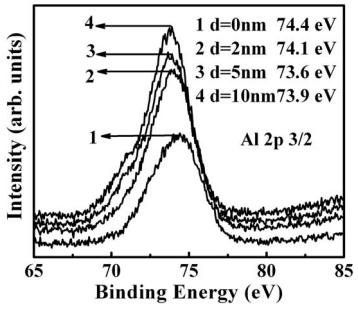

FIG. 6. XPS patterns of nanocapsules D with etching depths of 0, 2, 5, and 10 nm.

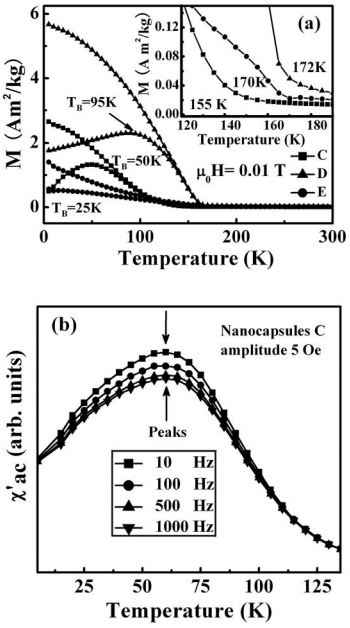

FIG. 7. (a) Zero-field-cooled and field-cooled magnetization curves of nanocapsules C–E between 5 and 300 K, at an applied field of 0.01 T; the detail of the magnetization curves in the inset shows different Curie temperatures of nanocapsules C–E. (b) The temperature dependence of ac susceptibility measured after the ZFC process.

B. Magnetic properties and magnetocaloric effect of $GdAl_2/Al_2O_3$ nanocapsules

The temperature dependences of the magnetization in nanocapsules C–E were measured in the zero-field-cooled (ZFC) and field-cooled (FC) processes between 5 and 300 K under a relatively low field of 0.01 T. From Fig. 7(a), the curves show the features of the magnetic nanoparticle system. The maximum appears on the ZFC curves at 50, 95, and 25 K, indicating the blocking temperatures of nanocapsules C, D, and E, respectively. Each FC curve departs with the corresponding ZFC curve at a temperature a little larger than the blocking temperature. Due to the fact that bulk $GdAl_2$ shows ferromagnetism below 172 K, $GdAl_2$ nanocapsules, with their diameters smaller than the size of a single domain, show the superparamagnetic properties indicated by the characteristics of the ZFC-FC curves. However, because the present nanocapsules were put so close to each other during the magnetic measurement, there might exist strong mutual magnetic interactions between randomly distributed particles, which would induce the particle system to be in a spin glass state because of the frustration effect. When the particle system is of the spin glass state, the FC curve is always flattened below blocking temperature and the ac-susceptibility peaks shift to high temperature with the increase of the frequency.[35–37] However, in the present systems, the FC curves in Fig. 7(a) increase with decreasing temperature below the blocking temperature T_B. Meanwhile, the temperature dependence of the ac susceptibility measured after ZFC [Fig. 7(b)] shows that the ac-susceptibility peaks are almost unchanged as the frequency increases from

10 to 1000 Hz. Moreover, the values of the Curie temperature extrapolated from the reciprocal dc susceptibility obtained from FC curves are −6.5, 12.44, and 4.9 K, respectively, which are much smaller than the corresponding values of systems having strong mutual interactions.[35] As a result, the present experimental results are different from the cases where the existence of the strong mutual interaction between magnetic nanoparticles leads to the system of the spin glass state.[35–37] Present results suggest that interactions between the $GdAl_2/Al_2O_3$ nanocapsules are very weak, because the nonmagnetic Al_2O_3 shells hinder the direct contact between the magnetic cores. The weak interactions will not be the most influential factor in changing the magnetization of the nanocapsules. The magnetic behavior of the $GdAl_2/Al_2O_3$ nanocapsules can be described by the classical superparamagnetic theory without particles' interactions.

According to the superparamagnetic theory,[38] the blocking temperature T_B can be described by $25k_BT=KV$, where KV is the anisotropy energy barrier; K and V are the effective anisotropy constant and the volume of the particle, respectively.[39,40] In the present system, the magnetocrystalline anisotropy constant K can be estimated by this formula using the parameters of nanocapsules C and D, with $T_B=50$ and 95 K and average diameters of 19 and 24 nm, respectively. The calculated values for the anisotropy constant K are 4.8×10^3 and 4.5×10^3 J m^{-3}, being almost equal, which are much smaller than those of cobalt (2.7×10^5 J m^{-3}) and Fe (5.4×10^4 J m^{-3}).[41] This indicates that the anisotropy energy barrier of the $GdAl_2/Al_2O_3$ nanocapsules is much lower than those of Co and Fe nanocapsules when they have the same particle volume. For the present $GdAl_2/Al_2O_3$ nanocapsules C–E prepared by arc-discharging Gd-Al alloys with different compositions, their anisotropy energy barriers can be determined by their average diameters.

The big turns on the overlapped curves of ZFC and FC indicate the Curie temperatures of the $GdAl_2/Al_2O_3$ nanocapsules C–E, which are lower than the corresponding Curie temperature of bulk $GdAl_2$. This reduction of the Curie temperature is attributed to the change of intrinsic magnetic behaviors caused by the size effect and surface effect of nanometer particles.[11] Furthermore, as shown in the inset of Fig. 7(a), among nanocapsules C–E, nanocapsules C has the lowest Curie temperature because more Al atoms in the $GdAl_2$ lattice lead to the decrease of the density of states $N(E_F)$ at the Fermi level.[20] On the other hand, nanocapsules D display a magnetization larger than that of nanocapsules C at the same temperature, because the Gd content in the former is larger than that in the latter according to EDS analysis. By contrast, the nanocapsules E have the largest Gd content but the lowest magnetization, due to the fact that the smallest barrier and smaller magnetic field energy make the particles' moments relax easily, which cannot be fixed along the magnetic field in the lower field; the oxygen content in sample E also is the greatest, suggesting the formation of Gd_2O_3.

The hysteresis loops of the $GdAl_2/Al_2O_3$ nanocapsules C at 5, 20, and 80 K, measured in the ZFC process, show the hysteretic characteristic in Fig. 8(a). The coercive forces are 17.6 and 9.6 kA m^{-1} at 5 and 20 K, and no coercive force can be observed at 80 K because the $GdAl_2/Al_2O_3$ nanocapsules are of superparamagnetic state. It is seen from the inset of Fig. 8(a) that the magnetization curve at 180 K represents the typical paramagnetic characteristic above the Curie temperature of the $GdAl_2/Al_2O_3$ nanocapsules. Therefore, the $GdAl_2/Al_2O_3$ nanocapsules show different magnetic behaviors in three temperature ranges between 5 and 300 K. In Fig. 8(b), the hysteresis loops at 5 K show the coercive forces 17.6, 23.2, and 10.5 kA m^{-1} for nanocapsules C, D, and E, respectively, which indicate that the magnitude of the anisotropy energy barriers can be judged as increasing with the sequence of E, C, and D, because the coercivity depends strongly on the anisotropy energy barriers below the blocking temperature.[42,43] When the interaction between the nanocapsules is nonexistent or very weak, the magnetic behavior of superparamagnetic nanocapsules is similar to that of the paramagnets, but the relaxation of the particles' moments must overcome the hindrance of its energy barrier KV. With decreasing temperature, the decreased thermal agitation energy k_BT cannot help the particles' moments more easily overcome the barrier to make the relaxation time of particles' moments longer. When the relaxation time of particles' mo-

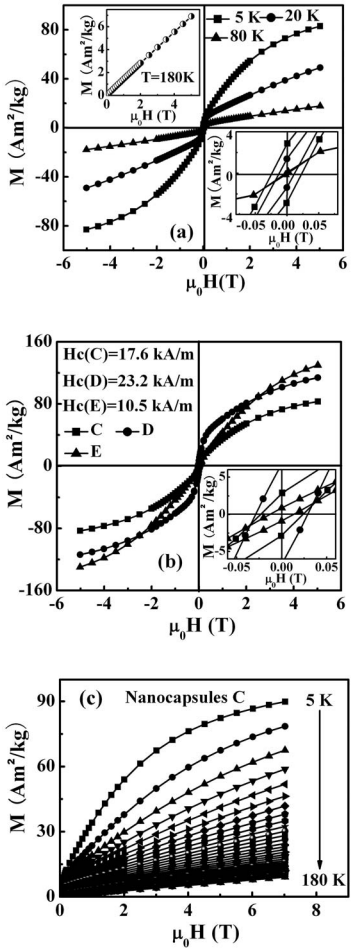

FIG. 8. (a) Hysteretic loops of nanocapsules C at 5, 20, and 80 K. The insets show the enlarged part and the magnetization curve of nanocapsules C at 180 K. (b) Hysteretic loops of nanocapsules C–E at 5 K and (c) the isothermal magnetization curves from 5 to 180 K in the ZFC process.

ments equals the measurement time of the measuring device, the temperature corresponding to the maximum in the ZFC magnetization curve under a lower field is called the blocking temperature.[38] Therefore, the scale of the energy barrier will determine the value of the blocking temperature. Also, below the blocking temperature, the relaxation time will be longer than the measurement time. Different from the superparamagnetic system, below blocking temperature, the relaxation of the particles' moments are hindered by the frustration effect coming from the strong interaction between the magnetic particles.

During the ZFC process, the isothermal magnetization curves were measured from 5 to 180 K with the interval of 5 K and at the applied field of 7 T [Fig. 8(c) for nanocapsules C]. At 5 K, the magnetization tends to the saturation and reaches 89.88 A m^2 kg^{-1}. With the average diameter of 20 nm of the spherical $GdAl_2$ core, the estimation of the Bohr magneton of the particle is about $4.9\times10^5\mu_B$; the theoretical value for the saturation magnetization of bulk $GdAl_2$ is about 205.42 A m^2 kg^{-1}. However, the magnetization measured for the present nanocapsules C, D, and E at 5 and 7 T are 89.88, 123.81, and 144.45 A m^2 kg^{-1}, respectively, which are about half of the $GdAl_2$ bulk value, which displays mainly the typical feature of a fine particle system.[35] The smaller magnetization of the present nanocapsules is also attributed to the fact that more substitution of nonmagnetic Al atoms and the nonmagnetic shells decrease the integral magnetization of nanocapsules C–E. On the other hand, in the low-temperature range, the large gap between the adjacent magnetization curves indicates the large change of magnetic order, which also suggests the large magnetic entropy change for the $GdAl_2/Al_2O_3$ nanocapsules.

According to the general thermodynamic equations, the entropy change of a magnetic system can be calculated from the thermodynamic Maxwell equation

$$\left(\frac{\partial S}{\partial H}\right)_T = \left(\frac{\partial M}{\partial T}\right)_H. \tag{1}$$

In the isothermal magnetizing process, the magnetic entropy change ΔS can be derived from Eq. (1) by integrating from initial field H_1 to the destination field H_2,

$$\Delta S(T,H) = \int_{H1}^{H2}\left(\frac{\partial M}{\partial T}\right)_H dH. \tag{2}$$

As the measurements were made with discrete field changes for each isotherm, we adopt the following numerical approximation:[44]

$$\Delta S\left(\frac{T_{n+1}+T_n}{2},H\right) = \sum\frac{M_{n+1}-M_n}{T_{n+1}-T_n}\Delta H. \tag{3}$$

Generally, in materials with blocking state, one cannot exploit the magnetocaloric effect from a magnetic field to zero field since the entropy is not well defined (because the magnetization value at zero field is not defined due to the fact that two different curves, i.e., the FC and ZFC, can be measured) and, in general, there is a drift in time of all the thermodynamic properties. However, one way to avoid this can be to define the entropy change between two states at finite values of the magnetic field, for instance, 7 and 1 T. According to Eq. (3), the magnetic entropy change ΔS of nanocapsules C–E between 5 and 180 K after a field variation from 1 to 7 T was calculated from the measurements of isothermal magnetization curves in Fig. 8(c). It is interesting to note that $-\Delta S$ increases continuously with the decrease of the temperature from 180 to 5 K. From the inset of Fig. 9(a), the temperature dependence of $d(-\Delta S)/dT$ shows that $-\Delta S$ increases rapidly at low temperatures, but smoothly above the blocking temperature. At 7.5 K, the $-\Delta S$ can reach the largest values of 18.02, 18.71, and 31.01 J kg^{-1} K^{-1} with the field variation from 1 to 7 T for nanocapsules C, D, and E, respectively. Apparently, the magnetic entropy change of the $GdAl_2/Al_2O_3$ nanocapsules at low temperature presents much larger values, which suggests that a large magnetization change $(\partial M/\partial T)_H$ will exist in the low temperatures at the given field change according to Eq. (2).[18] In addition, the temperature dependence of the magnetic entropy change in the present superparamagnetic $GdAl_2$ system is in agreement

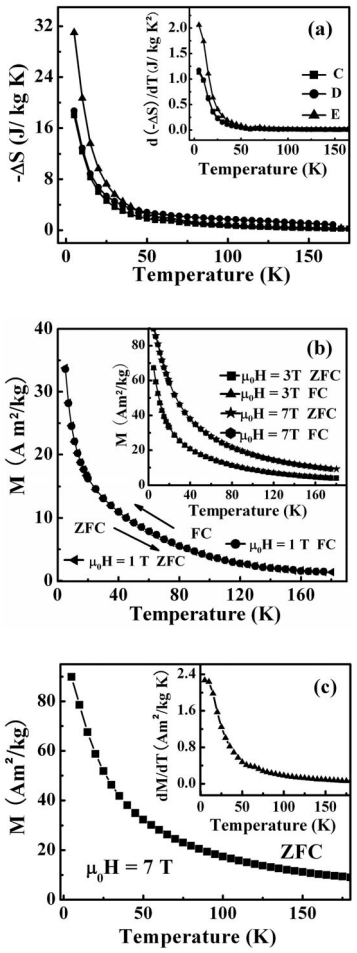

FIG. 9. (a) Temperature dependence of magnetic entropy change between 5 and 180 K of nanocapsules C–E at a field variation from 1 to 7 T. (b) Zero-field-cooled and field-cooled magnetization curves of nanocapsules C–E between 5 and 180 K, at applied fields of 1, 3, and 7 T. (c) Temperature dependence of magnetization of nanocapsules C in the zero-field-cooled process at the applied field of 7 T.

with the prediction about the temperature dependence of the entropy change for superparamagnetic-state isotropic nanoclusters.[18]

For traditional magnetic refrigeration materials, the large magnetic entropy change always appears near the transition temperature of the first-order magnetostructural change or second-order magnetic transition, near which the magnetic order will have large variation. Namely, the large $(\partial M/\partial T)_H$ value leads to the large magnetic entropy change. For the present $GdAl_2$ system, no magnetostructural variation and no second-order magnetic transition can be observed below their Curie temperatures, but the large magnetic entropy change appearing in the low-temperature range suggests the existence of a large $(\partial M/\partial T)_H$. Experimentally, we measured the temperature dependence of the magnetization, when the applied field was kept unchanged, to prove the existence of the large $(\partial M/\partial T)_H$.

Taking nanocapsules C as an example, the temperature dependence of magnetization at applied fields of 1, 3, and 7 T was plotted in Fig. 9(b). In Fig. 9(b), the ZFC and FC curves overlapped with each other exactly at the applied field of 1 T, which indicates that no irreversible behavior is present below the blocking temperature of nanocapsules C under the second applied field. Moreover, the ZFC and FC curves under larger applied fields of 3 and 7 T also indicate the magnetic reversible behavior between 5 and 180 K [see the inset of Fig. 9(b)]. As a result, the magnetic behavior of nanocapsules C in the ZFC and FC processes is equivalent, and the weak interaction between the nanocapsules will have almost no influence on the magnetization between 1 and 7 T. Figure 9(c) shows the ZFC curve of nanocapsules C between 5 and 180 K, and the variation of magnetization with decreasing temperature at an applied field of 7 T. It is clearly observed that the magnetization of the nanocapsules at 7 T decreases faster at lower temperatures and smoothly when the temperature tends to the Curie temperature, which can be further indicated by dM/dT [the inset of Fig. 9(c)]. According to the discussion above, the variation of the magnetization of the nanocapsules is determined by the applied field Zeeman energy, thermal agitation energy k_BT, anisotropy energy barrier, and weaker interaction energy between the particles, which have exciting and hindering effects on the rotation of the moments, respectively. With the change of thermal agitation energy k_BT, when the temperature is changed, the balance among the four kinds of energies will be broken, which will have different influences on the change of magnetization (change of magnetic order) in different temperature ranges.

For the assembly of the superparamagnetic $GdAl_2/Al_2O_3$ nanocapsules with random orientation, when the large external field was applied, the magnetization that is experimentally measured is determined by the sum of the projections of each individual particle's moment on the direction of the external magnetic field.[45,46] With the decrease of the effect on the rotation of the particles' moments agitated by the thermal exciting energy in low temperatures, more moments of the particles can rotate and fix on the direction of the external field, upon the effect of the applied field Zeeman energy, which increases the magnetization of the particle system. Then the balance forms among the applied field Zeeman energy, thermal agitation energy k_BT, anisotropy energy barrier, and weaker interaction energy between the particles. At the same time, because of the large magnetic-moment density of the $GdAl_2/Al_2O_3$ nanocapsules coming from the Gd atoms with a large atomic moment of $7.2\mu_B$, due to the presence of seven unpaired $4f$ electrons, which have a total angular momentum of $J=7/2$, the large magnetization was acquired at low temperatures. Consequently, when the temperature increases and the applied field changes, the balance is broken by the increase of the thermal energy and the decrease of the magnetic field Zeeman energy, and the particles' system will have a large magnetic entropy change caused by the large magnetization change because of the weak hindering effect on the rotation of the particles' moments by the smaller anisotropy barrier, coming from the anisotropy constant K (about 4.8×10^3 J m^{-3}) and small particle volume V, compared with that of Fe(C) nanocapsules.[47]

For N independent superparamagnetic nanoparticles with particle moments m, at an external field H and temperature T, their magnetic entropy change was calculated directly according to the Langevin theory,[8] where $y=mH/k_BT$, k_B is Boltzmann's constant, and M_0 is the saturation magnetization of the particles' system,

$$\frac{T\Delta S}{M_0H}=\frac{1}{y}\left[1-y\coth y+\ln\left(\frac{\sinh y}{y}\right)\right]. \tag{4}$$

When y has a definite value, the right part of Eq. (4) will be equal to a constant k, then

$$\Delta S=k\frac{M_0H}{T}. \tag{5}$$

Here, $-\Delta S$ scales with the reciprocal of the temperature $1/T$. To compare with the theoretical result, the correlations between $-\Delta S$ and $1/T$ in the $GdAl_2$ system with different size distributions and average diameters were plotted in Fig. 10(a). Although the existence of size distribution results in different particle magnetic moments m, which will not render y a constant, the linear relation between $-\Delta S$ and $1/T$ is kept, shown by the superparamagnetic $GdAl_2/Al_2O_3$ nanocapsules C and E in Fig. 10(a). Nevertheless, for the present sample D, the linear relation between $-\Delta S$ and $1/T$ is not kept, which suggests that a much wider size distribution can break this kind of linear relation.

Importantly, for nanocapsules C–E in the low-temperature range, ΔS is proportional to $1/T$, even though the wider size distribution in nanocapsules D cannot influence this linear relation, which indicates that the particles' size distribution is not the main factor in this linear relation at low temperatures. Then, according to the experimental data, at low temperatures, the $-\Delta S$ of the $GdAl_2/Al_2O_3$ nanocapsules can be simply described as

$$-\Delta S=\alpha\frac{1}{T}. \tag{6}$$

Taking nanocapsules C as an example, the $1/T$ dependence of $-\Delta S$ at different ΔH is shown in Fig. 10(b). With different ΔH, the linear relations between $1/T$ and $-\Delta S$ can be observed. In the inset of Fig. 10(b), the slope coefficient α

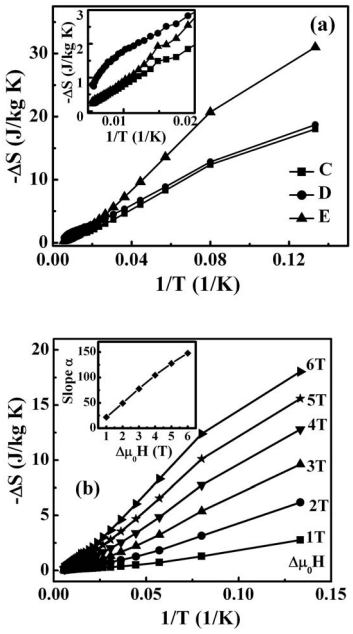

FIG. 10. The $1/T$ dependence of the magnetic entropy change (a) for nanocapsules C–E at a field change of 6 T and (b) for nanocapsules C with a field change from 1 to 7 T. The inset in (a) shows the details of the high-temperature range of (a), while the inset in (b) is the slope α at different ΔH for nanocapsules C.

linearly increases with an increase in ΔH, which leads to α that can be described as $\alpha = \beta \Delta H$. Then the magnetic entropy change $-\Delta S$ can be further described as

$$-\Delta S = \beta \frac{\Delta H}{T}, \tag{7}$$

where the coefficient β is a function of the energy barrier KV and the saturation magnetization of the $GdAl_2/Al_2O_3$ nanocapsules. Equation (7) is similar to Eq. (5) derived from Eq. (1). In essence, the magnetic entropy change of the $GdAl_2/Al_2O_3$ nanocapsules as a whole comes from the effect on the fluctuation of particle magnetization, when the change in applied field and temperature occurs. Because the relaxation of the moments of superparamagnetic $GdAl_2/Al_2O_3$ nanocapsules is similar to the relaxation of paramagnets, the appearance of the linear relation between $-\Delta S$ and $1/T$ is attributed to the paramagnetic relaxation mechanism, according to which Eq. (4) was deduced.

With the energy viewpoint, Eq. (5), deduced theoretically by McMichael *et al.*,[8] can be written as

$$T\Delta S = kM_0 H. \tag{8}$$

It suggests the conservation of the energy in the process of magnetic entropy change of the superparamagnetic particle system. Accordingly, for the present $GdAl_2/Al_2O_3$ nanocapsules, the conservation of the energy should also be obeyed in the process of producing a large magnetic entropy change at low temperatures. Equation (7) constructed experimentally can also be written as

$$-T\Delta S = \beta \Delta H, \tag{9}$$

where β corresponds to kM_0 in Eq. (8). When ΔH is constant in Eq. (7), the linear relation between $-\Delta S$ and $1/T$ can be valid. As a result, the physical meaning beyond the linear dependence of $-\Delta S$ with $1/T$ at low temperatures can also be described as follows: from the point of view of the conservation of energy, the isothermal magnetic entropy change $-\Delta S$ is determined by the variation of the Zeeman energy from the external applied field H_1 to H_2.

IV. SUMMARY

The intermetallic compound $GdAl_2/Al_2O_3$ nanocapsules have been prepared by the modified arc-discharge technique. The formation of $GdAl_2/Al_2O_3$ is controlled by the boiling points of different elements and initial contents of the elements in the anode. The morphologies of the $GdAl_2/Al_2O_3$ nanocapsules show an irregular spherical shape, and the typical core-shell structure with amorphous Al_2O_3 as shells and crystalline $GdAl_2$ as cores can be represented. The Curie temperatures of the $GdAl_2/Al_2O_3$ nanocapsules decrease with the increase of the substitutional Al atoms in the $GdAl_2$ lattice. The magnetic entropy change of the $GdAl_2/Al_2O_3$ nanocapsules gradually increases with decreasing temperature from 180 to 5 K, and the sharp enhancement is exhibited when the system is subjected to low temperatures. The appearance of the large entropy change for the $GdAl_2/Al_2O_3$ nanocapsules in low temperatures can be ascribed to the lower anisotropy energy barriers and higher magnetic moment densities. At low temperatures, the entropy change of the $GdAl_2/Al_2O_3$ nanocapsules was found to be perfectly linear, scaling with $1/T$, and the anisotropy energy barrier influences the slope of the lines.

ACKNOWLEDGMENTS

This work was supported by the National Natural Science Foundation of China under Grant No. 50331030. The authors thank W. J. Ren for helpful discussion.

[1] V. K. Pecharsky, K. A. Gschneidner, Jr., A. O. Pecharsky, and A. M. Tishin, Phys. Rev. B **64**, 144406 (2001).
[2] V. K. Pecharsky and K. A. Gschneidner, Jr., Phys. Rev. Lett. **78**, 4494 (1997).
[3] H. Wada and Y. Tanabe, Appl. Phys. Lett. **79**, 3302 (2001).
[4] F. X. Hu, B. G. Shen, J. R. Sun, and X. X. Zhang, Appl. Phys. Lett. **78**, 3675 (2001).
[5] T. Mazet, H. Ihou-Mouko, and B. Malaman, Appl. Phys. Lett. **89**, 022503 (2006).
[6] J. A. Barclay and W. A. Steyert, Cryogenics **22**, 73 (1982).
[7] M. E. Zhitomirsky, Phys. Rev. B **67**, 104421 (2003).
[8] R. D. McMichael, R. D. Shull, L. J. Swartzendruber, and L. H.

Bennett, J. Magn. Magn. Mater. **111**, 29 (1992).
[9] T. A. Yamamoto, M. Tanaka, T. Nakayama, and K. Niihara, Jpn. J. Appl. Phys., Part 1 **39**, 4761 (2000).
[10] T. A. Yamamoto, M. Tanaka, K. Shiomi, and K. Niihara, in *Nanophase and Nanocomposite Materials III*, MRS Symposia Proceedings No. 581, edited by S. Komarneni, J. C. Parker, and H. Hahn (Materials Research Society, Pittsburgh, 2000), p. 297.
[11] Y. Shao, J. X. Zhang, J. K. L. Lai, and C. H. Shek, J. Appl. Phys. **80**, 76 (1996).
[12] M. S. Pedersen, S. Mø´rup, S. Linderoth, and M. Hanson, J. Phys.: Condens. Matter **9**, 7173 (1997).
[13] T. Kinoshita, S. Seino, H. Maruyama, and T. A. Yamamoto, J. Alloys Compd. **364**, 281 (2004).
[14] R. D. Shull, R. D. McMichael, and J. J. Ritter, Nanostruct. Mater. **2**, 205 (1993).
[15] J. A. Nelson, L. H. Bennett, and M. J. Wagner, J. Am. Chem. Soc. **124**, 2979 (2002).
[16] R. D. McMichael, J. J. Ritter, and R. D. Shull, J. Appl. Phys. **73**, 6946 (1993).
[17] M. Evangelisti, A. Candini, A. Ghirri, and E. J. K. Mclnnes, Appl. Phys. Lett. **87**, 072504 (2005).
[18] X. X. Zhang, H. L. Wei, Z. Q. Zhang, and L. Zhang, Phys. Rev. Lett. **87**, 157203 (2001).
[19] K. H. J. Buschow, Rep. Prog. Phys. **42**, 1373 (1979).
[20] M. Magnitskaya, G. Chelkowska, G. Borstel, M. Neumann, and H. Ufer, Phys. Rev. B **49**, 1113 (1994).
[21] N. Kaplan, E. Dormann, K. H. J. Buschow, and D. Lebenbaum, Phys. Rev. B **7**, 40 (1973).
[22] M. Bauer, M. S. S. Brooks, and E. Dormann, Phys. Rev. B **48**, 1014 (1993).
[23] H. Kropp, E. Dormann, A. Grayevsky, and N. Kaplan, J. Phys. F: Met. Phys. **13**, 207 (1983).
[24] R. W. Teale, Y. Oner, and Z. P. Han, J. Phys.: Condens. Matter **1**, 3841 (1989).
[25] S. Ma, D. Y. Geng, W. S. Zhang, and Z. D. Zhang, Nanotechnology **17**, 5406 (2006).
[26] V. P. Dravid, J. J. Host, M. H. Teng, and J. R. Weertman, Nature (London) **374**, 602 (1995).
[27] K. A. Gschneidner, Jr., V. K. Pecharsky, and A. O. Tsokol, Rep. Prog. Phys. **68**, 1479 (2005).
[28] Z. D. Zhang, J. Mater. Sci. Technol. **23**, 1 (2007).
[29] X. L. Dong, Z. D. Zhang, Y. C. Chuang, and S. R. Jin, Phys. Rev. B **60**, 3017 (1999).
[30] S. Ma, Y. B. Wang, D. Y. Geng, and Z. D. Zhang, J. Appl. Phys. **98**, 094304 (2005).
[31] Z. D. Zhang, in *Encyclopedia of Nanoscience and Nanotechnology*, edited by H. S. Nalwa (American Scientific, California, 2004), Vol. 6, pp. 77–160.
[32] M. Z. Wu, Y. D. Zhang, S. Hui, and T. D. Xiao, J. Appl. Phys. **92**, 491 (2002).
[33] D. Y. Geng, Z. D. Zhang, W. S. Zhang, and X. P. Song, Scr. Mater. **48**, 593 (2003).
[34] D. Y. Geng, W. Y. Park, J. C. Kim, and Z. D. Zhang, J. Mater. Res. **20**, 2534 (2005).
[35] M. Garcia del Muro, X. Battle, and A. Labarta, J. Magn. Magn. Mater. **221**, 26 (2000).
[36] Y. Sun, M. B. Salamon, K. Garnier, and R. S. Averback, Phys. Rev. Lett. **91**, 167206 (2003).
[37] X. Batlle, M. Garcia del Muro, and A. Labarta, Phys. Rev. B **55**, 6440 (1997).
[38] X. X. Zhang, J. Tejada, J. M. Hernandez, and R. F. Ziolo, Nanostruct. Mater. **9**, 301 (1997).
[39] X. X. Zhang, J. M. Hernandez, J. Tejada, R. Sole, and X. Ruiz, Phys. Rev. B **53**, 3336 (1996).
[40] J. Tejada, R. F. Ziolo, and X. X. Zhang, Chem. Mater. **8**, 1784 (1996).
[41] Z. D. Zhang, J. L. Yu, J. G. Zheng, I. Skorvanek, J. Kovac, X. L. Dong, Z. J. Li, S. R. Jin, H. C. Yang, Z. J. Guo, W. Liu, and X. G. Zhao, Phys. Rev. B **64**, 024404 (2001).
[42] C. de Julian Fernandez, Phys. Rev. B **72**, 054438 (2005).
[43] F. C. Fonseca, G. F. Goya, R. F. Jardim, R. Muccillo, N. L. V. Carreno, E. Longo, and E. R. Leite, Phys. Rev. B **66**, 104406 (2002).
[44] L. H. Lewis, M. H. Yu, and R. J. Gambino, Appl. Phys. Lett. **83**, 515 (2003).
[45] M. Bode, O. Pietzsch, A. Kubetzka, and R. Wiesendanger, Phys. Rev. Lett. **92**, 067201 (2004).
[46] R. Prozorov, Y. Yeshurun, T. Prozorov, and A. Gedanken, Phys. Rev. B **59**, 6956 (1999).
[47] Z. D. Zhang, J. G. Zheng, I. Skorvanek, G. H. Wen, J. Kovac, F. W. Wang, J. L. Yu, Z. J. Li, X. L. Dong, S. R. Jin, W. Liu, and X. X. Zhang, J. Phys.: Condens. Matter **13**, 1921 (2001).